Inductance and Resistance Computations for Three-Dimensional Multiconductor Interconnection Structures

Ruey-Beei Wu, Chien-Nan Kuo, and Kwei K. Chang

Abstract—**A computer-aided analysis system has been established to calculate the equivalent inductance and resistance matrices for three-dimensional multiconductor interconnection structures. Based on the theory of partial element equivalent circuit, the interconnection structures are first decomposed into many straight segments which are of circular or rectangular cross sections but can be in arbitrary orientation. The resistances and partial inductances between all these segments are calculated using analytical integration and quadrature formulae. They are finally assembled into the desired equivalent impedance matrix by general network theory. Illustrative examples include the analysis for non-uniformly coupled transmission lines and the calculation for skin-effect impedances of transmission lines and three-dimensional structures. The numerical results are in good agreement with the measurement data and the available results in the literature.**

I. Introduction

With today's level of complexity in integrated technology, the consideration of computer package is as important as the circuit design [1]. As the switching of circuits becomes very fast, the interconnections can no longer be considered as ideal short lines but instead, circuit elements with resistances, capacitances and inductances [2]. The resultant signal delay, reflection, crosstalk, and distortion may degrade the system performance. The characterization of electrical parameters and the analysis of electrical properties for such interconnection structures become fundamental to system synthesis and optimization. To accurately determine the electrical parameters of the three-dimensional packaging structures, a capacitance analysis program had been developed [3], [4]. The present paper is devoted to the evaluation of equivalent inductances and resistances for arbitrary three-dimensional multiconductor interconnection structures.

The inductance plays a very important role in the electrical engineering applications. The computation formulae for basic structures such as straight filaments and coils have been extensively presented [5] (and the references therein). However, due to the complexity of geometry, the inductance computations for interconnection systems are usually hard to access by analytical method or direct integration. Ruehli *et al.* thus proposed a general and systematic method of partial element equivalent circuit (PEEC) to deal with this problem [6], [7]. They decomposed the interconnection system into a lot of parallel or orthogonal straight segments for the calculation of partial inductances and from which, extracted the desired equivalent inductances. Later, based on a similar idea, Kamikawai *et al.* considered the three-dimensional inductance of finite-length transmission lines [8]. The present paper generalizes the PEEC method by allowing the modeling of inclined and arbitrarily oriented line segments. The evaluation of partial inductances and resistances and the extraction of equivalent impedances for this more general analysis are discussed here. Also, several illustrative examples are presented to verify and demonstrate some novel applications of the method.

Manuscript received February 6, 1991; revised September 17, 1991. This work was supported in part by grants from the Electronics Research and Service Organization and the National Science Council of the Republic of China.

R.-B. Wu and C.-N. Kuo are with the Department of Electrical Engineering, National Taiwan University, Taipei, Taiwan, R.O.C.

K. K. Chang is with the Electronics Research and Service Organization, Industrial Technology Research Institute, Hsin-Chu, Taiwan, R.O.C.

IEEE Log Number 9104780.

II. PEEC Method

To begin with, consider a general N-loop system as shown in Fig. 1. Under the assumption of uniform current distribution across the cross sections of the conductors, the mutual inductance between loops i and j can be given by [6]

$$L_{ij} = \frac{1}{a_i a_j} \frac{\mu}{4\pi} \oint_i \int_{a_i} \oint_j \int_{a_i} \frac{d\hat{l}_i \cdot d\hat{l}_j}{r_{ij}} da_i \, da_j. \quad (1)$$

Here, $\mu = 4\pi$ nH/cm is the permeability of the free space, r_{ij} denotes the distance between two points in the two conductors, while the integration is taken over the cross sectional areas da_i and da_j and along the current flow directions $d\hat{l}_i$ and $d\hat{l}_j$ of conductors i and j, respectively. The self inductance can be found from (1) by letting $i = j$.

In fact, the application of (1) is very limited since the numerical evaluation for the multiple integral requires tremendous computation time. A better approach is to decompose the loops into straight segments, say that the loops i and j are divided into K and M elements, respec-

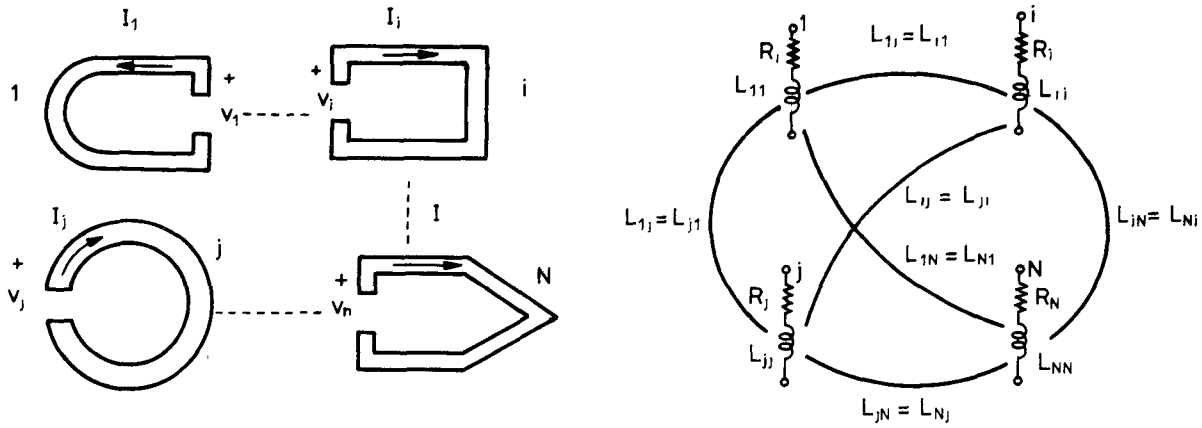

(a) (b)

Fig. 1. An N-loop interconnection structure and its equivalent circuit.

tively. Between every two segments, it is advantageous to define the partial inductance [6]

$$L_{p_{km}} = \frac{1}{a_k a_m} \frac{\mu}{4\pi} \int_{a_k} \int_{a_m} \int_{b_k}^{c_k} \int_{b_m}^{c_m} \frac{d\hat{l}_k \cdot d\hat{l}_m}{r_{km}} da_k\, da_m \quad (2)$$

where b_k, c_k and b_m, c_m denote the two ends of the kth and mth segments, respectively. Then, the loop integrals (1) can be restored from the assembly of these partial inductances, i.e.,

$$L_{ij} = \sum_{k=1}^{K} \sum_{m=1}^{M} S_{km} \cdot L_{p_{km}} \quad (3)$$

where the sign S_{km} is $+1$ or -1 depending on whether the loop currents in the two segments are in similar or in reverse directions. If the two segments are orthogonal to each other, the partial mutual inductance $L_{p_{km}}$ is zero.

III. Evaluation of Partial Inductances

A. Partial Self Inductances

In the evaluation of partial inductances, we must compute the self inductance for each segment and the mutual inductance between any two segments. The self inductance depends on the segment length and the cross sectional shape. Most of the practical structures can be decomposed into straight segments which are of circular or rectangular cross section. For circular segments with length l and radius ρ, the self inductance can be found by [9]

$$\frac{L}{l} = \frac{\mu}{8\pi} + \frac{\mu}{2\pi} \cdot \left[\ln \left(\frac{l}{\rho} + \sqrt{1 + \frac{l^2}{\rho^2}} \right) - \sqrt{1 + \frac{\rho^2}{l^2}} + \frac{\rho}{l} \right]. \quad (4)$$

For rectangular segments, let the length be l and the widths of two sides be W and T, respectively. Defining the normalized widths $w = W/l$, $t = T/l$, and the normalized distances

$$r = \sqrt{w^2 + t^2}, \quad \alpha_w = \sqrt{w^2 + 1}, \quad \alpha_t = \sqrt{t^2 + 1},$$
$$\alpha_r = \sqrt{w^2 + t^2 + 1},$$

the self inductance given in (2) can be written as [6]

$$\begin{aligned} \frac{L}{l} = \frac{2\mu}{\pi} \Bigg\{ & \frac{1}{4} \left[\frac{1}{w} S\left(\frac{w}{\alpha_t}\right) + \frac{1}{t} S\left(\frac{t}{\alpha_w}\right) + S\left(\frac{1}{r}\right) \right] \\ & + \frac{1}{24} \left[\frac{t^2}{w} S\left(\frac{w}{t\alpha_t(r + \alpha_r)}\right) + \frac{w^2}{t} S\left(\frac{t}{w\alpha_w(r + \alpha_r)}\right) \right. \\ & + \frac{t^2}{w^2} S\left(\frac{w^2}{tr(\alpha_t + \alpha_r)}\right) + \frac{w^2}{t^2} S\left(\frac{t^2}{wr(\alpha_w + \alpha_r)}\right) \\ & \left. + \frac{1}{wt^2} S\left(\frac{wt^2}{\alpha_t(\alpha_w + \alpha_r)}\right) + \frac{1}{tw^2} S\left(\frac{tw^2}{\alpha_w(\alpha_t + \alpha_r)}\right) \right] \\ & - \frac{1}{6} \left[\frac{1}{wt} T\left(\frac{wt}{\alpha_r}\right) + \frac{t}{w} T\left(\frac{w}{t\alpha_r}\right) + \frac{w}{t} T\left(\frac{t}{w\alpha_r}\right) \right] \\ & - \frac{1}{60} \left[\frac{(\alpha_r + r + t + \alpha_t)t^2}{(\alpha_r + r)(r + t)(t + \alpha_t)(\alpha_t + \alpha_r)} \right. \\ & + \frac{(\alpha_r + r + w + \alpha_w)w^2}{(\alpha_r + r)(r + w)(w + \alpha_w)(\alpha_w + \alpha_r)} \\ & \left. + \frac{(\alpha_r + \alpha_w + 1 + \alpha_t)}{(\alpha_r + \alpha_w)(\alpha_w + 1)(1 + \alpha_t)(\alpha_t + \alpha_r)} \right] \\ & - \frac{1}{20} \left[\frac{1}{r + \alpha_r} + \frac{1}{\alpha_w + \alpha_r} + \frac{1}{\alpha_t + \alpha_r} \right] \Bigg\} \end{aligned} \quad (5)$$

where

$$S(x) \equiv \sinh^{-1}(x) = \ln(x + \sqrt{1 + x^2})$$

and $T(x) \equiv \tan^{-1}(x)$ denote the arc hyperbolic sine and arc tangent functions, respectively. At the filament approximation (T, $W \ll l$), the lengthly expression can be replaced by the empirical formula [5, p. 21]

$$\frac{L}{l} \cong \frac{\mu}{2\pi}\left[\ln \frac{2l}{0.2235 \cdot (W+T)} - 1\right]. \tag{6}$$

B. Partial Mutual Inductances

On the other hand, the partial mutual inductance depends mainly on the relative geometrical position and the lengths of the two segments and only slightly on the cross sectional shapes. Hence, to a first order approximation, we may calculate the filament inductances by assuming that the cross sectional sizes of the two segments are much smaller than the segment lengths and the distance. Under this filament approximation, arbitrary two segments in the three-dimensional space can be categorized into three classes: parallel, coplanar inclined, and more general, inclined in different planes. The analytical formulae of the filament mutual inductances for all these cases are available in the literature [5, ch. 6, 7].

The accuracy of the filament approximation depends much on the ratio of cross sectional size to segment distance. Consider two parallel segments of the same width W, thickness T, length l, and center-to-center distance D. After a tedious algebraic manipulation by applying the laws of summation of inductance [5, ch. 6], it is verified that the mutual inductance for this case can be given analytically by

$$M = \left[\frac{1}{2}(L_{D+T} + L_{D-T}) - L_D\right] \cdot \left(\frac{D}{T}\right)^2 + (L_{D+T} - L_{D-T}) \cdot \left(\frac{D}{T}\right) + \frac{1}{2}(L_{D+T} + L_{D-T}) \tag{7}$$

where the self inductances in RHS of (7) are calculated by (5) with the subscript denoting the thickness of the segment, whose width is W and length is l. Given the exact formula (7), the relative error of the filament approximation versus the ratio W/D for the case $T/W = 1$ are shown by the solid curves in Fig. 2 with the arrow denoting the decrease of parameter $D/l = 3$, 1, .3 and .1, accordingly. Roughly speaking, the error of filament approximation is proportional to the square of the W/D ratio. To assure the relative error within 1%, 0.1%, and 0.01% for various D/l, the W/D ratio must be smaller than 0.35, 0.11, 0.035, respectively. In common cases, the W/D ratio is larger than 0.035 such that the relative error is larger than 0.01%. To improve the accuracy, we may choose several filaments and find their weighted average by suitable quadrature formulae.

Since the cross sections of interest are circular or rectangular, only the following three combinations as shown in Fig. 3 need to be considered. For the first combination

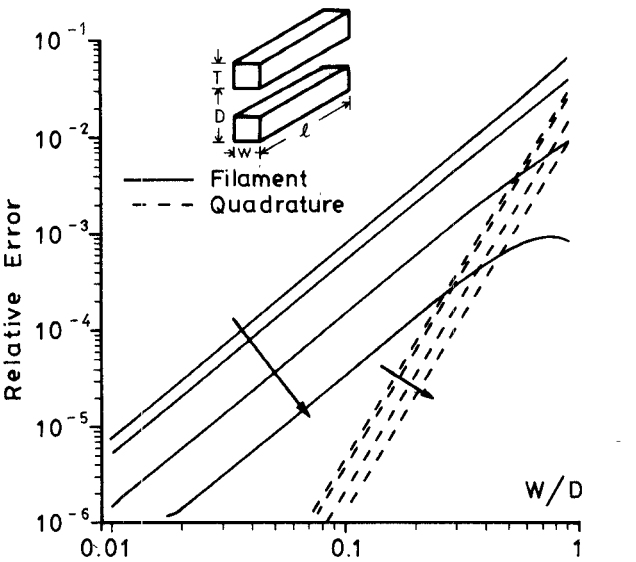

Fig. 2. Relative errors of calculated partial mutual inductance versus the W/D ratio. The sold and dashed curves denote the results obtained by filament and quadrature formula, respectively. The arrows indicate the decrease of the parameter $D/l = 3$, 1, 0.3, and 0.1 accordingly.

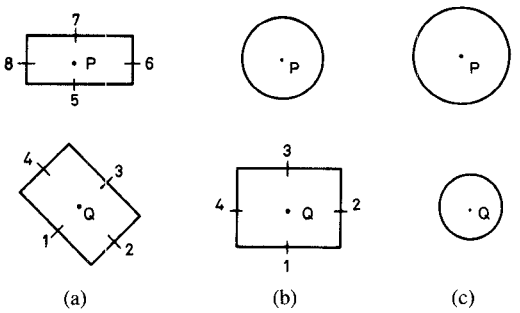

Fig. 3. Quadrature formulae for the mutual inductance between two segments that (a) both are rectangular, (b) one is circular and the other is rectangular, and (c) both are circular.

that both segments are rectangular, we choose five filaments as shown in Fig. 3(a) at each of the cross section. The mutual inductance can be found by the Rayleigh quadrature formula [5, p. 11]

$$M \cong \tfrac{1}{6}(M_{P1} + M_{P2} + M_{P3} + M_{P4} + M_{Q5} + M_{Q6} + M_{Q7} + M_{Q8} - 2 \cdot M_{PQ}). \tag{8}$$

where M_{P1} is the inductance between filaments P and 1, M_{Q5} is the inductance between filaments Q and 5, etc. The accuracy can be greatly improved by the quadrature formulae. For example, consider the aforementioned structure and calculate the mutual inductances by the quadrature formulae. As shown by the dashed curves in Fig. 2, the relative error is now proportional to the fourth power of the W/D ratio. Hence, to assure the relative error with 0.01% requires that the W/D ratio is smaller than 0.21, which is usually the case for practical structures.

To keep a similar accuracy, suitable quadrature formulae are required for the other two combinations in Fig. 3. For the combination shown in Fig. 3(b) that one is cir-

cular and the other is rectangular, the quadrature formula becomes

$$M \cong \tfrac{1}{6}(M_{P1} + M_{P2} + M_{P3} + M_{P4} + 2 \cdot M_{PQ}). \quad (9)$$

For the third combination shown in Fig. 3(c) that both segments are circular, the filament inductance M_{PQ} between the two center points P and Q is just enough for the desired mutual inductance M. Usually, the results by the above quadrature formulae are much more accurate than the filament approximation.

IV. Evaluation of Partial Resistances

The resistance calculations can be treated by the PEEC approach, of course much more simply. Since there is no mutual resistance between two conductor segments, only the partial resistance R_p of each segment need be considered. For a straight segment, the resistance can be found easily by

$$R_p = l/(\sigma \cdot A_{\text{eff}}) \quad (10)$$

where σ is the conductivity, l is the segment length, and A_{eff} is the effective cross sectional area.

At high frequencies, the current may crowd into the portions near the surface of the segment, the so-called skin effect. As a result, the effective area in (10) decreases such that the resistance suffers from a dramatic increase. To account for this effect, the current density $J(\vec{r})$ is assumed exponentially decaying along the radial direction of the cross section [10]. By neglecting the nonuniformity of the current along the periphery of conductor surface, or the so-called proximity effect [11], the effective area in (10) is then approximated by the formula

$$A_{\text{eff}} = \frac{\left|\iint J(\vec{r})\, da\right|^2}{\iint |J(\vec{r})|^2\, da} \cong \frac{\left|\iint e^{-(1+j)\epsilon(s)}\, da\right|^2}{\iint e^{-2\epsilon(s)}\, da} \quad (11)$$

where $\epsilon(s) = d(s)/\delta$ is the radial distance measured from the surface normalized to the skin depth $\delta = 1/\sqrt{\pi\mu\sigma f}$. At very low frequencies, the skin depth δ is much larger than $d(s)$ such that (11) can be reduced to the actual area.

Equations (10) and (11) can then be employed to evaluate the partial self resistances of the basic segments. For circular segments, the distance function $d(s) = \rho - s$ and the incremental area $da = 2\pi s\, ds$. Hence, the effective area is given by

$$A_{\text{eff}} = 2\pi\rho\delta \cdot \left|1 - \frac{1 - e^{-\gamma\epsilon}}{\gamma\epsilon}\right|^2 \Big/ \left[1 - \frac{1 - e^{-2\epsilon}}{2\epsilon}\right] \quad (12)$$

or $A_{\text{eff}} \cong \pi\rho^2 \cdot (1 - \epsilon^2/9)$ if $\epsilon \ll 1$, where $\gamma = 1 + j$ and $\epsilon = \rho/\delta$. For rectangular segments, we choose T the length of the shorter side and model that $d(s) = T/2 - s$ and $da = 2 \cdot [2s + (W - T + 2s)]\, ds$. Then, the effective area in (10) can be given by

$$A_{\text{eff}} = 2(W + T)\,\delta \cdot \left|1 - \frac{1 - \alpha}{1 + \alpha} \cdot e^{-\gamma\epsilon} - \frac{2\alpha}{1 + \alpha} \cdot \frac{1 - e^{-\gamma\epsilon}}{\gamma\epsilon}\right|^2 \Big/ \left[1 - \frac{1 - \alpha}{1 + \alpha} \cdot e^{-2\epsilon} - \frac{\alpha}{1 + \alpha} \cdot \frac{1 - e^{-2\epsilon}}{\epsilon}\right] \quad (13)$$

or

$$A_{\text{eff}} \cong WT \cdot [1 - \epsilon^2 \cdot (3 - \alpha^2)/18] \quad \text{if } \epsilon \ll 1,$$

where

$$\gamma = 1 + j, \quad \alpha = T/W \quad \text{and} \quad \epsilon = T/2\delta.$$

V. Equivalent Impedance Matrix

It is difficult to apply (3) directly to calculate the inductances in common packaging structures, where the complexity usually allows no simple loops to be identified. Nonetheless, the equivalent impedances between any two interconnection nodes of interest can be extracted from the partial inductances and resistances by applying the general network theorem. Let $[V_b]$ and $[I_b]$ denote the vectors consisting of the voltage drops and the currents, respectively, along all the conductor segments, or the so-called branches. Then, they can be related in s domain by

$$[V_b] = ([R_p] + s[L_p]) \cdot [I_b] \equiv [Z_p] \cdot [I_b] \quad (14)$$

where the diagonal matrix $[R_p]$ is made of the partial resistances while the matrix $[L_p]$ is made of the partial inductances.

All the nodes in the interconnection system can be categorized into several groups, among each of which the nodes can be linked physically. Choosing one node as the voltage reference among each group, we can define for each node the nodal voltage V_n and the net current I_n flowing into the node. According to the well-known Kirchhoff's current law (KCL) and voltage law (KVL), the nodal voltages and currents can be related to the branch voltages and currents by

$$[A] \cdot [I_b] = [I_n] \quad \text{and} \quad [A]^T \cdot [V_n] = [V_b]. \quad (15)$$

Here, $[A]$ is the so-called incidence matrix of the partial circuit, which in the convention is such that $A_{ib} = 1$ and $A_{jb} = -1$ when the current in branch b flows from node i to j. The superscript T denotes the matrix transpose. Note that the group references are excluded from the node list in the incidence matrix.

Substituting (15) into (14), it can be shown that the nodal voltages and currents satisfy the relation

$$[I_n] = ([A] \cdot [Z_p]^{-1} \cdot [A]^T) \cdot [V_n]. \quad (16)$$

Usually, only few of the nodes are chosen as the output terminals. For all other internal nodes, the net nodal currents are zero. By a similar derivation, it can be shown that the voltages and currents of the output terminals, $[V_O]$

and $[I_O]$, satisfy

$$[V_O] = [Z_{eq}] \cdot [I_O];$$

$$[Z_{eq}] = [B]^T \cdot ([A] \cdot [Z_p]^{-1} \cdot [A]^T)^{-1} \cdot [B] \quad (17)$$

given the incidence matrix B of the output equivalent circuit. Here, $[Z_{eq}]$ is the desired equivalent impedance matrix between the output terminals.

In the computation of equivalent impedance matrix, the inner loop in the parenthesis of (17) calls for a matrix inversion and two matrix multiplications. It is noted that the resultant matrix $[X]$ from the multiplication of matrices $[Z_p]^{-1}$ and $[A]^T$ can be obtained more directly by solving the matrix equation

$$[Z_p] \cdot [X] = [A]^T. \quad (18)$$

Then, the computation for the inner loop $[X'] = [A] \cdot [Z_p]^{-1} \cdot [A]^T$ calls for a matrix equation solution and a matrix multiplication only. Similar approach can be applied to simplify the computation for the outer loop operation $[B]^T \cdot [X']^{-1} \cdot [B]$.

Since there is no mutual inductance between two orthogonal segments as given by (2), the matrix $[Z_p]$ usually consists of many zero off-diagonal elements. Suitably renumbering the segments, all the nonzero elements can be flocked to the positions near the matrix diagonal. For practical interconnection structures, all the segments are categorized into five kinds, i.e., Z, X, Y, S, and G lines according to their direction of current flow. The X, Y, and Z lines are parallel to the x, y, and z axes, while the S and G lines stand for the inclined lines parallel to the x-y plane and the general three-dimensional lines, respectively. Then, only the mutual inductance between two segments in the following eleven combinations need be considered. They are Z-Z, X-X, Y-Y, which belong to parallel segments, X-S, Y-S, S-S, which are coplanar inclined, and Z-G, X-G, Y-G, S-G, G-G, which are inclined in different planes. To take advantage of the sparsity in $[Z_p]$, the Z lines are numbered first and then X, S, Y, and G lines accordingly. The matrix elements are stored in the skyline representation, while the matrix equation in (18) is solved efficiently by the LU-factorization [12]. Both the computer memory and computation time are thus reduced substantially.

VI. Numerical Results

Based on the PEEC approach, a computer-aided analysis system has been tailored on IBM/PC to calculate the inductances and resistances for arbitrary three-dimensional interconnection structures. Also, a graphic input interface is set up to facilitate the specification and verification of the structure geometry. The output equivalent impedances are stored according to the convention of SPICE and are ready for next-step circuit simulation and analysis. In its present version, the program can deal with up to about 120 conductor segments in less than one minute on a PC/AT-386 with the 387 coprocessor. Of course, the program can be ported to larger computers for the analysis of complicated structures with more conductor segements.

To check the validity of the present approach, the first example considers a structure formed by multiple connected loops shown in Fig. 4(a), which is made of circular cooper wire having radius 0.5 mm. The loop impedance is measured by the RLC meter in the frequency range 20 kHz to 10 MHz. Due to the presence of the branches, no simple loop can be identified to apply the traditional inductance formula (1). The PEEC approach becomes unique here since it can handle arbitrary interconnections. The calculated resistance and inductance are shown by solid and dashed curves in Fig. 4(b), respectively. The triangular marks denoting the experimental data are also shown in the figure for comparison.

It is noted that the calculated inductance slightly decreases from its low frequency limit to its high frequency limit. There is good agreement between the calculated and measured inductances, with less than 7% deviation. In this case, the nonuniform current distribution due to the skin effect has a negligible influence on the inductance, since the cross sectional size of the conductors is small compared with the distance between conductors. On the other hand, the resistance increases significantly versus the frequency due to the skin effect. The comparison between the calculated and measured resistances is reasonable at low or middle frequencies, but worse at higher frequencies. The discrepancy may be contributed to the fact that the reactance ωL becomes much larger than the resistance R at high frequencies, which makes the measured resistance less reliable.

When the conductors are very close to each other, the inductance may vary quite a bit with the frequency due to both the skin and proximity effects at high frequencies [11], [13]. The assumption of uniform current distribution will result in a noticeable error in the calculation inductance. Nonetheless, the present approach can deal with the effects by further dividing the cross section of the conductor segment into small cells [11]. Inside each cell, the current distribution is assumed uniform with an unknown constant. These constants may be different from cell to cell and will be solved by applying the aforementioned general network theorem. Good results will be achieved by this modeling technique if the size of the cells, especially those near the periphery of the conductor, is kept smaller than the skin depth at the desired frequency.

For example, consider a transmission line formed by two rectangular conductors of size $2a \times 2b$ and center-to-center distance $2c$. The triangular and square marks in Fig. 5 show the calculated results for the case that $a = 1$, $b = 0.1$, $c = 0.5$ mm and $a = b = 1$, $c = 2$ mm, respectively. The solid and dashed curves are obtained by a two-dimensional boundary integration equation analysis [13]. It is found that the present results are satisfactory in the low or middle frequency range. At a high frequency say $f = 10$ MHz, the skin depth $\delta \cong 0.021$ mm becomes much smaller than the cross section such that each conductor should be divided into hundreds of cells to achieve

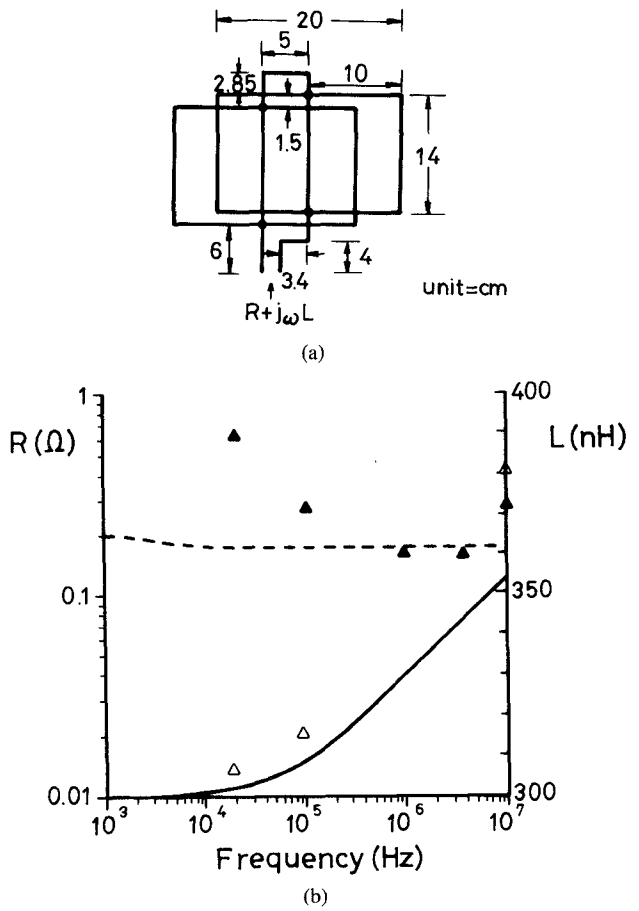

Fig. 4. Equivalent impedance versus frequency for a complicated loop. The solid and dashed curves denote the calculated resistance and inductance, respectively. The triangular marks are experimental data.

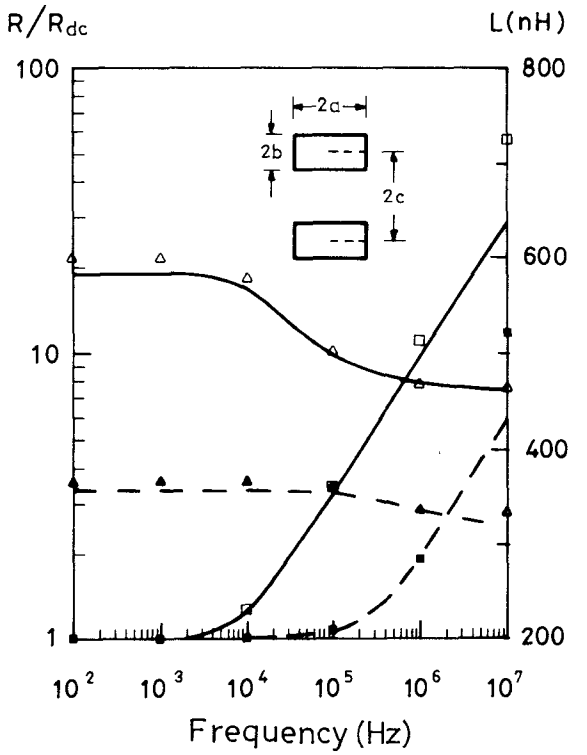

Fig. 5. Skin effect resistance and inductance for a transmission line formed by two rectangular conductors. The hollow square and triangular marks denote the calculated resistance and inductance, respectively, for the case that $a = b = 1$, $c = 2$ mm. Similarly, the solid marks are for the cae that $a = 1$, $b = 0.1$, $c = 0.5$ mm. They are compared with the two solid and dashed curves obtained by a boundary integral equation analysis [13].

satisfactory results. The number of unknowns increases dramatically and the numerical computation becomes too time-consuming.

The next example considers two coupled transmission lines over a ground plane as shown in Fig. 6(a). When the center-to-center distances d_1 and d_2 at the two ends are different, the coupling is non-uniform. As far as the high-frequency inductances are concerned, we need only model the current distribution along the conductor surface. In the following analysis, each transmission line is further divided into 16 segments along the periphery of cross section, three along each narrow side and five along each wide side. On the other hand, based on the image theory, the presence of ground plane is modeled by including two image conductors under the ground plane as shown in Fig. 6(b). The program calculates the two loop inductances L for a given length l and the mutual inductance M in between. At the limit that l tends to infinity, the inductance matrix of the coupled transmission line system can be given by $L_{11} = L_{22} = \frac{1}{2}L/l$ and $L_{12} = L_{21} = \frac{1}{2}M/l$, while the inductive coupling coefficients is $k_L = M/L$.

Table 1 lists the numerical results versus various lengths l for three cases with uniform distance $d = d_1 = d_2 = 12$, 18, and 24, respectively, and one nonuniform case with

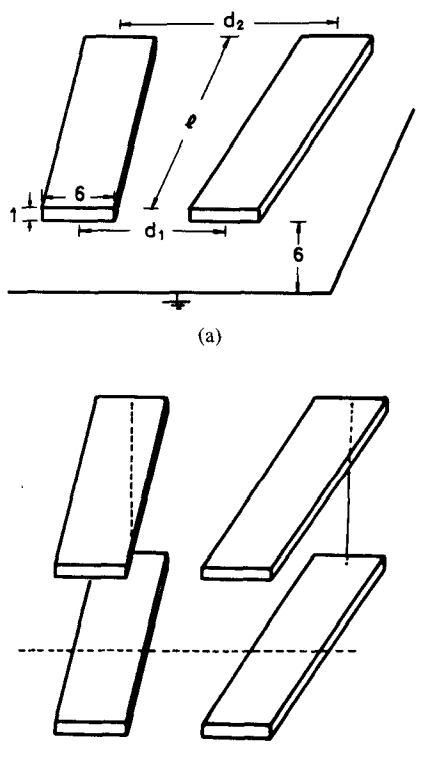

Fig. 6. Inductance calculations for nonuniformly coupled transmission lines. (a) original structure, and (b) equivalent structure by image theory.

TABLE I
INDUCTANCE MATRIX FOR THE COUPLED TRANSMISSION LINES SHOWN IN FIG. 6

l (mil)	$d_1 = d_2 = 12$		$d_1 = d_2 = 18$		$d_1 = d_2 = 24$		$d_1 = 12, d_2 = 24$	
	$\frac{1}{2}L/l$	$\frac{1}{2}M/l$	$\frac{1}{2}L/l$	$\frac{1}{2}M/l$	$\frac{1}{2}L/l$	$\frac{1}{2}M/l$	$\frac{1}{2}L/l$	$\frac{1}{2}M/l$
20	2.971	.4537	2.988	.1895	2.990	.0936	3.201	.1879
50	3.429	.6470	3.454	.3018	3.458	.1630	3.490	.3234
100	3.610	.7370	3.639	.3615	3.643	.2049	3.647	.3911
200	3.707	.7877	3.737	.3965	3.742	.2312	3.737	.4301
500	3.766	.8200	3.797	.4200	3.803	.2488	3.796	.4553
1000	3.786	.8311	3.818	.4280	3.823	.2500	3.816	.4639
2000	3.797	.8369	3.828	.4320	3.834	.2581	3.826	.4683
5000	3.803	.8400	3.835	.4345	3.840	.2601	3.833	.4709
∞	3.803	.8417	3.834	.4357	3.840	.2611	—	—

The unit is nH/cm.

$d_1 = 12$ and $d_2 = 24$. It is found that the per unit-length inductances increase, and so is coupling coefficient, versus the length l and finally approach a constant value. The coupling coefficient k_L in the non-uniform case ($d_1 = 12$, $d_2 = 24$) lies somewhat between those in the two uniform cases with $d = 12$ and 24, respectively. To the first order aproximation, the value is close to k_L in the uniform case with $d = (d_1 + d_2)/2 = 18$.

Conventionally, the inductance matrix for ideal uniformly coupled transmission lines system is obtained from the inverse of its two-dimensional capacitance matrix in homogeneous environment [14]. Here, the results based on the conventional approach are listed in the last row marked by $l = \infty$. It is verified that the conventional approach can give satisfactory inductances in the two-dimensional limit. However, the present three-dimensional inductance analysis is inevitable in investigating practical transmission lines with finite length or nonuniform coupling.

The last example illustrates the inductance modeling of multilayer ceramic (MLC) structures used for multichip packaging in a high-performance computer system [15]. Consider a simplified off-chip interconnection path between the driver and receiver as shown in Fig. 7(a). The output terminals C and E are used as the dual power supply in bipolar circuits, R as the signal reference, and S as the signal. When the switching signal propagates from S_1 to S_2, the package inductance causes a ΔI noise between the power supply terminals of the driver, which then propagates down to the receiver [16]. It is thus of concern to find the equivalent inductances shown in Fig. 7(b) between these output terminals of the package. However, the package structure contains so many branches that the current loops can hardly be defined. Furthermore, the current loops are incomplete until the devices are connected to the output nodes. Nonetheless, the PEEC method gives an equivalent inductance matrix between all the output nodes, as listed in Table II. After including the device models of the chips and the signal connection, the equivalent inductance matrix can be put into the circuit simulation for the detailed noise analysis.

For example, the current during the switching can be assumed to flow from C_1 to S_1, via the signal line to S_2, shorted to T_2, then via the package and a large capacitance between T_g and C_g, and again via the package back to C_1. In ac operation, the large capacitance between T_g and C_g can be simply modeled by an electrically short. Hence, the effective inductance of the package to this current flow

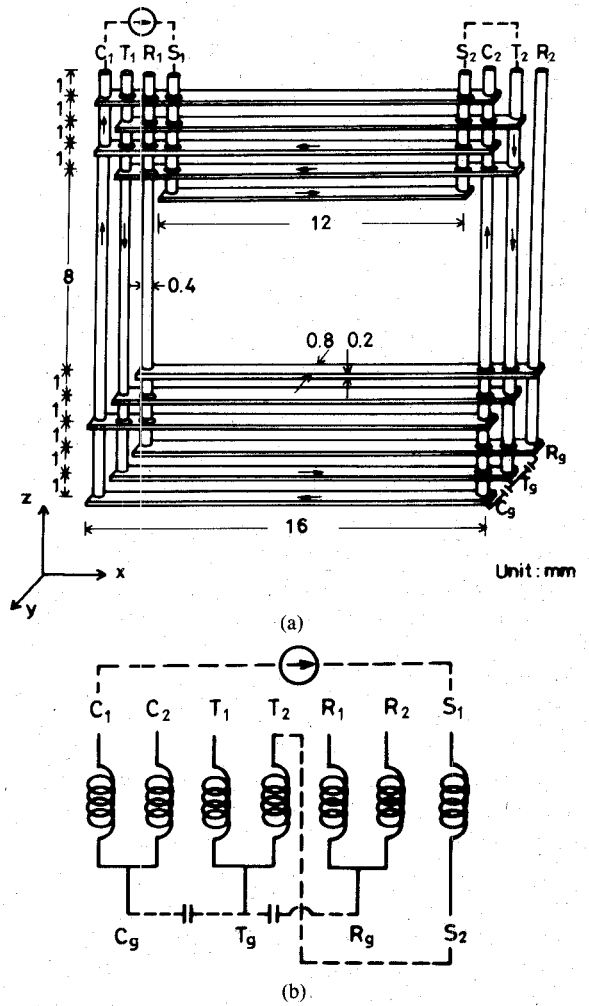

Fig. 7. Inductance modeling of a simplified multi-layer structure. (a) Original structure. (b) Equivalent circuit.

TABLE II
EQUIVALENT INDUCTANCE MATRIX FOR THE MULTILAYER STRUCTURE IN FIG. 7

	$C_1 - C_g$	$C_2 - C_g$	$T_1 - T_g$	$T_2 - T_g$	$R_1 - R_g$	$R_2 - R_g$	$S_1 - S_2$
$C_1 - C_g$	13.594	7.421	9.124	4.309	7.513	3.207	2.790
$C_2 - C_g$	(.619)	10.584	4.312	6.277	3.512	4.445	−1.773
$T_1 - T_g$	(.677)	(.362)	13.380	6.515	8.846	3.801	3.671
$T_2 - T_g$	(.367)	(.606)	(559)	10 142	4.068	5.657	−1.486
$R_1 - R_g$	(.496)	(.263)	(.589)	(.311)	16.870	3.396	4.096
$R_2 - R_g$	(.263)	(.414)	(.315)	(.538)	(.250)	10.910	−1 060
$S_1 - S_2$	(.203)	(−.146)	(.269)	(−.125)	(.267)	(−.086)	13.930

The unit of inductance is nH The numbers in the parenthesis denote the mutual inductance coefficients.

will be

$$L_{\text{eff}} = L_{C_1 - C_g} + L_{S_1 - S_2} + L_{T_2 - T_g} - 2M_{C_1 - C_g, S_1 - S_2} - 2M_{C_1 - C_g, T_2 - T_g} + 2M_{S_1 - S_2, T_2 - T_g} \cong 20.5 \text{ nH}.$$

In other words, when the current switching rate if $\Delta I/\Delta t = 10$ mA/ns, the total ΔI noise between C_1 and S_1 will be 205 mV. Among them,

$$\Delta V_{C_1} = (-L_{C_1 - C_g} + M_{C_1 - C_g, S_1 - S_2} + M_{C_1 - C_g, T_2 - T_g}) \cdot \Delta I/\Delta t \cong -65 \text{ mV}$$

will present at the chip pad C_1 with respect to the reference C_g. Similarly, the noise voltages will be −29.2, 10.6, 43.5, 6.5, 13.9, and 140 mV at the chip pads C_2, T_1, T_2, R_1, R_2, and S_1, respectively.

VII. Conclusion and Discussion

A general inductance and resistance analysis system has been set up to deal with arbitrary three-dimensional interconnection structures. The calculated results are in good agreement with the measured data and the available results in the literature. The system is very useful if only the structure of interest is small in size compared with the wavelength at the operating frequency. Several novel applications are also exploited in this paper, such as the investigation of the inductive coupling between two nonuniformly coupled transmission lines and the evaluation of the ΔI noise in a multi-layer computer packaging structure.

The most fundamental assumption in the present approach is the uniform current distribution inside the cross section of each conductor segment in the inductance computation. It is found that the calculated results are satisfactory for most practical structures where the cross sectional size of the conductor is much smaller than the distance between them. Only under the cases that the conductors are very close to each other and the frequency is high, this assumption may result in noticeable error. Even so, this difficulty can be alleviated somewhat by dividing the cross section into smaller cells. Of course, the number of unknowns may increase dramatically at high frequencies such that the numerical computation becomes very time-consuming.

Acknowledgment

The authors would like to thank Mr. S. Y. Yu, Mr. F. L. Chao, Mr. C. S. Hsu, Mr. C. J. Pang, Mr. H. J. Lee, and Dr. S. K. Jeng for their helpful discussion and technical assistance.

References

[1] E. E. Davidson and G. A. Katopis, "Package electrical design," in *Microelectronics Packaging Handbook*, R. R. Tummala and E. J. Rymaszewski Eds., New York: Van Nostrand Reinhold, 1989, ch. 3.
[2] A. E. Ruehli, "Survey of computer-aided electrical analysis of integrated circuit interconnections," *IBM J. Res. Develop.*, vol. 23, pp. 626-639, Nov. 1979.
[3] R. B. Wu and L L. Wu, "Exploiting structure periodicity and symmetry in capacitance calculations for three-dimensional multiconductor systems," *IEEE Trans. Microwave Theory Tech.*, vol. 36, pp. 1311-1318, Sept. 1988.
[4] R. B. Wu, "Interperiod capacitance calculations for three-dimensional multiconductor systems," *IEEE Trans. Microwave Theory Tech.*, vol. 36, pp. 1515-1520, Nov 1988.
[5] F. W. Grover, *Inductance Calculations: Working Formulas and Tables*. New York: Van Nostrand, 1962.
[6] A. E. Ruehli, "Inductance calculation in a complex integrated circuit environment," *IBM J. Res. Develop.*, vol. 16, pp. 470-481, Sept. 1972.
[7] P. A. Brenan, N. Raver, and A. E. Ruehli, "Three-dimensional inductance computations with partial element equivalent circuits," *IBM J. Res. Develop.*, vol. 23, pp. 661-668, Nov. 1979.
[8] R. Kamikawai, M. Nishi, K. Nakanishi, and A. Masaki, "Electrical parameter analysis from three-dimensional interconnection geometry," *IEEE Trans. Comp., Hybrids, Manuf. Technol.*, vol. CHMT-8, pp. 269-274, June 1985.
[9] A. J. Rainal, "Computing inductive noise of chip packages," *AT&T Bell Lab. Tech. J.*, vol. 63, pp. 177-195, Jan. 1984.
[10] J. D. Jackson, *Classical Electrodynamics*, 2nd ed., New York: Wiley, 1975, sec. 8.1, pp. 335-339.
[11] W. T. Weeks, L. L. Wu, M. F. McAllister, and A. Singh, "Resistive and inductive skin effect in rectangular conductors," *IBM. J. Res. Develop.*, vol. 23, pp. 652-660, Nov. 1979.
[12] K. J. Bathe and E. L. Wilson, *Numerical Methods in Finite Element Analysis*. Englewood Cliffs, NJ: Prentice-Hall, 1976, ch. 7.
[13] R. B. Wu and J. C. Yang, "Boundary integral equation formulation of skin effect problems in multiconductor transmission lines," *IEEE Trans. Magn.*, vol. 25, pp. 3013-3015, July 1989.
[14] W. T. Weeks, "Calculation of coefficients of capacitance of multiconductor transmission lines in the presence of a dielectric interface," *IEEE Trans. Microwave Theory, Tech.*, vol. MTT-18, pp. 35-43, Jan. 1970.
[15] B. T. Clark and Y. M. Hill, "IBM multichip multilayer ceramic modules for LSI chips - design for performance and density," *IEEE Trans. Comp., Hybrids, Manuf. Technol.*, vol. CHMT-3, no. 1, pp. 89-93, Mar. 1980.
[16] G. A. Katopis, "Delta-I noise specification for a high-performance computing machine," *Proc. IEEE*, vol. 73, no. 9, pp. 1405-1415, Sept. 1985.

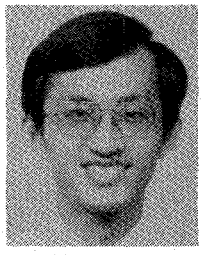

Ruey-Beei Wu was born in Tainan, Taiwan, Republic of China, on October 27, 1957. He received the B.S.E.E. and Ph.D. degrees from National Taiwan University, Taipei, Taiwan, in 1979, and 1985, respectively.

In 1982, he joined the faculty of the Department of Electrical Engineering, National Taiwan University, where he is now a Professor. In 1986, he was a Visiting Scientist for one year in IBM General Technology Division laboratory, East Fishkill Facility, Hopewell Junction, NY. He works primarily on the applications of numerical methods to electromagnetic field problems. He has been engaged in research on dielectric waveguides, optical fibers, wave scattering of anisotropic objects, edge slot antennas, microstrip discontinuities, and interconnection modeling for computer packaging.

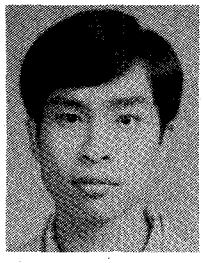

Chien-Nan Kuo received the B.S. degree in electronic engineering from National Chiao-Tung University, Hsin Chu, Taiwan, and the M.S. degree in electrical engineering from National Taiwan University, Taipei, Taiwan, in 1988 and 1990, respectively.

He is presently serving in the military. His research includes the simulation and characterization for the electric performance of electronic packaging.

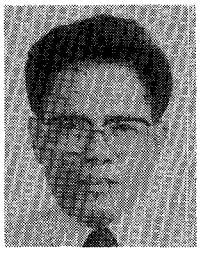

Kwei K. Chang was born in China on December 24, 1940. He received the B.S.M.E. degree from National Taiwan University, Taipei, Taiwan, in 1964, and the Ph.D. degree in physics from University of South Carolina, Columbia, SC in 1974.

From 1977 to 1984 he was an Assistant Professor of the Department of Mechanical Engineering and Aerospace Sciences at University of Central Florida, Orlando, FL. From 1984 to 1985 he was a member of the Technical Staff at Rockwell International, NAAO, Los Angeles, CA, where he was engaged in the analysis of IR signature and propagation and jet fighter fuel cooling. From 1985 to 1986 he was a member of the Technical Staff at TRW Space & Technology, Redondo Beach, CA where his primary work was on the modeling of optical phase conjugation cells. From 1986 to 1987, he was with LESO Consultant Corp. where his main project was related to laser scintillation effects. In 1987, he joined Electronic Research & Service Organization of Industrial Technology Research Institute in Hsin Chu, Taiwan, where presently he is a Researcher in the Division of Electronic Packaging Technology. His research areas have been in microwave and interconnection theory, conductor transmission & EMI simulations, stress characterization for multichip modules, and neural networks.